

Evidence of Impulsive Heating in Active Region Core Loops

Durgesh Tripathi, Helen E. Mason

*Department of Applied Mathematics and Theoretical Physics, University of Cambridge,
Wilberforce Road, Cambridge CB3 0WA, UK*

and

James A. Klimchuk

NASA Goddard Space Flight Center, Greenbelt, MD20771, USA

d.tripathi@damtp.cam.ac.uk

ABSTRACT

Using a full spectral scan of an active region from the Extreme-Ultraviolet Imaging Spectrometer (EIS) we have obtained Emission Measure $EM(T)$ distributions in two different moss regions within the same active region. We have compared these with theoretical transition region EMs derived for three limiting cases, namely *static equilibrium*, *strong condensation* and *strong evaporation* from Klimchuk et al. (2008). The EM distributions in both the moss regions are strikingly similar and show a monotonically increasing trend from $\log T[\text{K}] = 5.15\text{--}6.3$. Using photospheric abundances we obtain a consistent EM distribution for all ions. Comparing the observed and theoretical EM distributions, we find that the observed EM distribution is best explained by the *strong condensation* case (EM_{con}), suggesting that a downward enthalpy flux plays an important and possibly dominant role in powering the transition region moss emission. The downflows could be due to unresolved coronal plasma that is cooling and draining after having been impulsively heated. This supports the idea that the hot loops (with temperatures of 3–5 MK) seen in the core of active regions are heated by nanoflares.

Subject headings: Sun: corona — Sun: atmosphere — Sun: transition region — Sun: UV radiation

1. Introduction

Solar coronal heating has been one of the most intensely studied problems in solar physics over the past 60 years. Despite major advances in the observational and theoretical tools, the solution remains elusive (see e.g., Klimchuk 2006). Active regions provide a target of opportunity to study the dominant heating mechanisms for the corona. The basic building blocks of active regions are coronal loops. Because of the lack of cross-field transport of mass and thermal energy in the corona, the problem of coronal heating can effectively be reduced to a clear understanding of the heating mechanism in a single isolated coronal loop or loop strand.

The large-scale 1 MK loops and fan-like loops (which appear at the periphery of active regions) are seen clearly in observations recorded using the Transition Region and Coronal Explorer (TRACE; Handy et al. 1999) 171 Å passband. Their properties appear to be consistent with impulsive heating models (see e.g., Tripathi et al. 2009; Warren, Winebarger, and Mariska 2003; Klimchuk 2006, 2009, and references cited therein). However, the 3–5 MK loops in the core of the active regions are more diffuse and more difficult to isolate even with present day observatories. Hence it is more difficult to measure the physical plasma parameters along these hot core loops and to compare those properties with simulated results (although see López Fuentes and Klimchuk 2010). The "moss" regions are located at footpoints of hot (3–5 MK) loops (Martens et al. 2000; Antiochos et al. 2003; Tripathi et al. 2010) and they map the photospheric magnetic flux very closely (Tripathi et al. 2008). The moss regions, being the footpoints of the hot loops, provide a unique opportunity to study the dominant heating mechanism at work in active region core loops.

A number of publications involving observational results, analytical and 1D numerical simulations have proposed that steady heating is at play in the hot loops associated with moss regions. The main argument is that minimal variability is observed in brightness of the moss emission or in the Doppler shifts and line widths of spectral lines. Antiochos et al. (2003) pointed out that impulsive heating would produce transient loops in the cores of active regions that would be seen by *TRACE* as the plasma cools through 1 MK. Such loops are present but not ubiquitous. The authors also noted that the brightness of moss is quite steady when averaged over several *TRACE* pixels. Brooks and Warren (2009) later showed that Doppler shifts and line widths observed by the Extreme ultraviolet Imaging Spectrometer (EIS) on *Hinode* are also quite steady. Finally, Tripathi et al. (2010) measured the density and thermal properties of moss observed by EIS and found that they do not change significantly over periods ranging from an hour to 5 days.

These observations provide compelling evidence that heating in the cores of active regions must be quasi-steady *if* the cross-field scale of the heating is comparable to the 2 arcsec

(1.5 Mm) resolution of EIS or larger. That is, we can conclude that the heating is steady, but only if the plasma does not have unresolved sub-structure. There is good reason to believe that such sub-structure may exist, however (e.g., Klimchuk 2006). Individual thin strands could be highly time variable, and yet an unresolved bundle would appear steady as long as the strands are not in phase. This is true for both the coronal portions of the strands and their moss footpoints.

We therefore seek a diagnostic of heating that does not require that the fundamental structures be resolved. Doppler shifts are one possibility. Steady heating tends to produce no Doppler shift because the loop evolves to a static equilibrium (although see Mariska and Boris 1983; Klimchuk et al. 2010). Impulsive heating would produce a net red shift on the other hand. In an unresolved bundle of strands, some strands would have upflows due to evaporation and others would have downflows due to condensation (cooling and draining). Simulations show that the upflows are faster, fainter, and shorter lived than the downflows (Patsourakos and Klimchuk 2006). Hence, the composite line profile would be red shifted by several kilometers per second, and very hot lines would also have a faint blue wing enhancement. The red shifts are predicted to decrease with temperature and may even become blue shifts in the hottest lines (Bradshaw and Klimchuk 2010, in preparation). The observational picture concerning Doppler shifts in moss regions is unclear. Some published measurements indicate minimal red-shifts consistent with steady heating (e.g., Brooks and Warren 2009), while other measurements indicate larger red-shifts consistent with impulsive heating (e.g., Doschek et al. 1976; Brueckner 1981; Klimchuk 1987; Doschek et al. 2008; Del Zanna 2008). This is an important area of future work.

Another diagnostic of coronal heating that works when there is unresolved sub-structure is the emission measure distribution, $EM(T)$, or the closely related differential emission measure distribution, $DEM(T)$. Since the plasma is roughly isothermal along the coronal portion of a strand, $EM(T)$ in the corona is determined primarily by the distribution of strand temperatures. An isothermal corona with all strands having the same temperature implies steady heating (Warren 1999; Landi et al. 2002), but some coronal $EM(T)$ support a nanoflare interpretation (e.g., Patsourakos and Klimchuk 2009; O’Dwyer et al. 2010; Reale et al. 2009). Warren et al. (2010) suggested that the lack of a strong correlation between hot and warm emission in the core of an active region is evidence that the heating must be steady. We disagree that this is the only interpretation. The relative intensities of coronal emission formed at, say, $\log T = 6.0$ and 6.5 can vary greatly depending on the magnitude of the nanoflares (e.g., Klimchuk et al. 2008, Figs. 4 and 7, dashed curves).

Moss is the transition region footpoints of hot strands, and the $EM(T)$ there is determined largely by the variation of temperature along the strands. Klimchuk et al. (2008) have

shown that the form of $EM(T)$ is different under three limiting conditions: *static equilibrium*, *strong condensation* and *strong evaporation*. We make use of these differences in the work reported here. We measure the EM distribution of two moss regions observed by EIS and compare them to the theoretical predictions. In this way we distinguish between steady and impulsive heating.

The rest of the paper is structured as follows. In section 2 we present our observations. In section 3 we provide the emission measure expressions following Klimchuk et al. (2008). Section 4 provides results and we summarise and discuss our results in section 5.

2. Observations

In this study, we have analysed observations recorded by the EIS aboard Hinode. The EIS instrument observes the spectral ranges 170–210 and 250–290 Å, providing observations in a broad range of temperatures ($\log T[\text{K}] = 4.7\text{--}7.3$). For detailed information on EIS see Culhane et al. (2007). For most of the EIS studies only a limited number of spectral lines were chosen due to the limitations on telemetry. However, occasionally full spectral scans of specific regions have been telemetered. Here we use one such raster of an active region AR 10961 recorded on July 01, 2007 at 03:18 UT. The active region first appeared on the east limb on June 26th, 2007. The data analysed were obtained from a single raster that scanned a field of view (FOV) of 128'' by 128'' with the 1'' slit, moving from west to east with an exposure time of 25 sec. The over-plotted box on the *TRACE* 171 Å image displayed in the left panel of Fig. 1 marks the region which was rastered by EIS. An EIS image obtained in Fe XII $\lambda 195.12$ Å is shown in the right panel of Fig. 1.

The full spectral scan allowed us to choose spectral lines formed over a broad range of temperature, which is essential in order to obtain a good EM distribution of the plasma. This is the first time a full spectral scan is being used to derive an EM distribution in active region moss. In our study we have used relatively clean spectral lines (see Table 1) with temperatures of formation $\log T[\text{K}] = 5.1\text{--}6.5$ based on EIS spectral atlases (Landi and Young 2009; Young and Landi 2009). The standard EIS software provided in *SolarSoft* were used to process the data and *eis_auto_fit*, also provided in *SolarSoft*, was used for Gaussian fitting the spectral lines. To de-blend some of the blended lines labelled 'b' in Table 1 we have used the same procedure as in Tripathi et al. (2010) based on the suggestions of Young et al. (2007, 2009).

We have derived EM following the approach of Pottasch (1963) whereby individual emission lines yield estimates of the emission measure at the lines' temperatures of formation.

Table 1: Spectral lines used to study the emission measure distribution in moss regions.

Ion	Wavelength [Å]	log T [K]
O IV	279.6	5.15
O IV	279.9	5.15
O V	248.5	5.35
O VI	183.9	5.45
O VI	184.1	5.45
Mg V	276.6	5.45
Si VI	246.0	5.60
Fe VIII	185.2	5.60
Mg VI	269.0	5.65
Mg VII ^b	278.4	5.80
Si VII	275.3	5.80
Fe IX	171.1	5.85
Fe X	184.5	6.05
Si IX	258.1	6.05
Si X	261.0	6.15
Fe XI	180.4	6.15
Fe XI	188.3	6.15
Fe XII	192.4	6.20
Fe XII	193.5	6.20
Fe XII ^b	195.1	6.20
Fe XIII	202.0	6.25
Fe XIV ^b	274.2	6.30
Fe XV	284.2	6.35
Fe XVI	263.0	6.45
Ca XIV	193.8	6.55

An EM distribution is built up by considering lines formed over a wide range of temperatures. The method requires the contribution function to be approximated by a function such that it is defined to be a constant over the temperature range $\log T_{\max} - 0.15$ to $\log T_{\max} + 0.15$ where T_{\max} is the temperature where the contribution function has its maximum. A detailed description of this method is given in Tripathi et al. (2010).

3. Theoretical Transition Region Emission Measure

Klimchuk et al. (2008) derived the differential emission measure (DEM) distribution of the transition region of a strand in the limiting cases of strong evaporation (Equation A3), strong condensation (Equation A7), and static equilibrium (Equation A12). The transition region is taken here to be the region of steep gradient at the strand footpoints. Its temperature ranges from a chromospheric value up to approximately one-half of the maximum temperature in the strand. Thus, it can reach several MK for strands which are very hot. In the case of static equilibrium, a downward heat flux from the corona powers the radiative losses from the transition region. These losses are ignorable in the case of strong evaporation, where a downward heat flux drives an evaporative upflow. The energy flux of the upflow is dominated by enthalpy if the flow is subsonic. For the final case of strong condensation, the enthalpy of a downflow powers the transition region radiation, with the heat flux being relatively unimportant. See Bradshaw (2008) and Bradshaw and Cargill (2010a,b) for detailed discussions of the importance of downflows in heating the transition region and cooling the corona.

The expressions given in Klimchuk et al. (2008) are for the differential emission measure. The conversion to emission measure (EM) requires that they be multiplied by temperature and by $\ln(10)$, giving

$$EM_{se} \approx \ln(10) \left(\frac{\kappa_0}{14} \right)^{1/2} \frac{\bar{P} T^{3/4}}{k \Lambda(T)^{1/2}} \dots \textit{static equilibrium} \quad (1)$$

$$EM_{con} \approx -\ln(10) \frac{5 k J_0 T}{\Lambda(T)} \dots \textit{strong condensation} \quad (2)$$

$$EM_{ev} \approx \frac{\ln(10)}{20} \frac{\kappa_0}{k^3} \frac{\bar{P}^2 T^{1/2}}{J_0} \dots \textit{strong evaporation} \quad (3)$$

where $\kappa_0=1.0 \times 10^{-6}$ in cgs units, k is Boltzmann's constant, T is temperature. J_0 is mass flux defined as $J_0 = nv$, where n and v are electron number density and plasma flow speed

respectively. \bar{P} is average pressure along a strand. $\Lambda(T)$ is the optically thin radiative loss function. Fig. 2 displays the radiative losses as a function of temperature calculated with CHIANTI (Dere et al. 1997) by free-free, radiative recombination and by line radiation for photospheric abundances (dashed-dotted line) of Grevesse and Sauval (1998) and coronal abundances (solid line) of Feldman (1992). For this calculation, we have used the CHIANTI v6.0.1 ionization equilibrium (Dere et al. 2009). The above equations give the emission measure curves for individual loop strands. While computing the theoretical EMs to compare with the observed EMs, we have considered the average pressure (\bar{P}) and mass flux J_0 as arbitrary constants. We have restricted ourselves to the temperature dependence of EM_{ev} , EM_{con} and EM_{se} and compared the shapes of the theoretical EM curves with those derived observationally as explained in section 2. The assumption of constant pressure and constant mass flux in a given strand is justified so long as the different parts of the solar atmosphere are connected along the magnetic field. However, this assumption would break down if plasma in different layers of the atmosphere were physically in different structures as was suggested by e.g., Landi and Feldman (2008) and references therein.

4. Results

Figure 3 displays EM curves for two different moss regions labelled "A" and "B" in the right panel of Fig. 1. The EM curves are created using the photospheric abundances (top panel) of Grevesse and Sauval (1998) and the coronal abundances (bottom panel) of Feldman (1992). The error bars on the EMs are computed by considering a 30% error in the observed intensities for all the spectral lines, which is a rough estimate of the cumulative errors due to radiometric calibration, line fitting and atomic calculations.

The EM curves for the two different regions displayed in Fig. 3 are very similar to each other when the same abundances are used. However, for a given region the EM curves are significantly different for the two different abundances, mainly at lower temperatures. The difference in the trend of the EM curves is basically due to the three data points on the extreme left, corresponding to three Oxygen lines namely O IV, O V and O VI. The EMs for Oxygen lines do not appear to be consistent with the EMs for other lines when coronal abundances are used. However, this discrepancy disappears when we use photospheric abundances. From the figure we note that the EMs of the Oxygen lines do not change when coronal or photospheric abundances are used. However, for other lines, the EMs increased by a factor of four for photospheric abundances, which makes the EMs for other lines consistent with the EMs for the Oxygen lines. Therefore, it seems appropriate to conclude that the composition in these moss regions is photospheric. However, we note that

Oxygen is the only element in our dataset with a high first ionization potential (FIP). The high-FIP O VI lines agree with the low-FIP Mg V line at $\log T = 5.4$ only with photospheric abundances. To verify the conclusion that moss regions must have photospheric abundances, it is important to examine additional pairs of high-FIP and low-FIP lines formed at the same temperature.

The observational picture of abundances in the solar upper atmosphere is not well established (see Feldman and Widing 2003, for a recent review). Using observations recorded by Skylab SO82A, it was found that in newly emerging active regions the composition was nearly photospheric. However, within a few hours after their emergence the composition starts to modify and it approaches a typical coronal composition (see Sheeley 1995; Widing 1997; Widing and Feldman 2001). Using data from the Coronal Diagnostic Spectrometer (CDS) aboard the Solar and Heliospheric Observatory (SoHO), Young and Mason (1997) found photospheric composition in an emerging flux region. The active region studied here had emerged about 6 days prior to the date when the data analysed here were recorded. Considering the results obtained using the Skylab observations, our analysis should suggest coronal abundances. It is worth mentioning, however, that Skylab SO82A was a slitless spectrometer which produced overlapping spectroheliograms providing partial information for active regions. Del Zanna (2003) suggested that the previous results based on Skylab observations overestimated the FIP bias by a large factor for active regions, if the plasma is isothermal rather than multi-thermal. Furthermore, since the moss regions are presumably confined to a relatively low altitude in the solar atmosphere, the FIP effect might not be significant in these regions. Therefore, photospheric abundances could prevail in moss regions.

The EM curves for the moss regions show that the peak of the emission comes from Fe XIII ($\log T = 6.25$) as suggested by Tripathi et al. (2010). In addition, the $EM(T)$ obtained using photospheric abundances shows a monotonic increase at lower temperatures from $\log T = 5.15$. However, the $EM(T)$ obtained using coronal abundances shows a minimum in the emission measure at $\sim \log T = 5.5$ similar to the EM curve obtained using the DEM distribution derived from SERTS EUV spectrum using the same abundances (Brosius et al. 1996, 2000).

We have compared the observed EM distributions obtained using coronal and photospheric abundances with those predicted theoretically for the three limiting cases of *static equilibrium* (EM_{se} , Eq. 1), *strong condensation* (EM_{con} , Eq. 2) and *strong evaporation* (EM_{ev} , Eq. 3) for both the regions 'A' and 'B' marked in the right panel of Fig. 1. Fig. 4 displays the observational EMs obtained using photospheric abundances over-plotted with the theoretical EMs for the three limiting cases, both for region 'A' and region 'B' in the left and right columns respectively.

The theoretical curve that provides the best overall match with the observed points is EM_{con} i.e., the strong condensation case (see plots in the middle row in Fig. 4). The EM_{se} for static equilibrium matches quite well with observed EM for temperatures below 1 MK but not at higher temperatures. However, that for strong condensation (EM_{con}) matches quite well for $\log T = 5.2 - 6.25$. Above $\log T = 6.3$, the EM_{con} suggests an increasing trend, whereas the observational EM starts to decrease. We can understand this apparent discrepancy as follows.

Suppose that unresolved strands are heating impulsively to very high temperatures by nanoflares and subsequently cooling. As stated earlier, the transition region in a given strand extends to roughly one-half of the maximum strand temperature. Recently heated strands will therefore contribute to moss emission over a wide range of temperatures, while strands that have cooled will only contribute emission at lower temperatures. We can imagine a collection of curves like those in the middle panels of Fig. 4 except truncated at different temperatures above $\log T = 6.3$. The sum of those curves would have a shape similar to the observed $EM(T)$, rolling over at $\log T = 6.3$. This basic effect can be seen in the transition region of model 4 in Klimchuk et al. (2008, Fig. 7, dot-dashed curve). The figure shows $DEM(T)$ ($= EM(T)/T$) and is therefore flat rather than positively sloped at the lower temperatures. The temperature where $EM(T)$ is expected to roll over will depend upon the number distribution and brightness of strands in different stages of cooling. Strands which have cooled below 1 MK should be relatively faint due to mass draining and therefore will have a reduced contribution to the composite $EM(T)$.

The EM_{ev} curve for strong evaporation does not show any resemblance to the observed EM curve. This is not surprising, since, in the nanoflare scenario, evaporative upflows are much fainter and much shorter lived than the subsequent condensation downflows and therefore contribute minimally to the net emission.

When using coronal abundances, we did not find a reasonable correspondence between the observed $EM(T)$ and any of the theoretical $EM(T)$. However, this conclusion is based on the disagreement in the emission measure at $\log T < 5.45$, and therefore depends entirely on EM of Oxygen lines. The EM_{con} and EM_{se} curves fit the data equally well in this questionable range $\log T < 5.45$. However, we note that at $\log T > 5.45$ EM_{con} provides a better fit to the data than EM_{se} regardless of which abundance set is assumed.

5. Summary and discussion

We have obtained EM distributions in active region moss using full spectral scans recorded with EIS for two different regions. The EM distributions for the two regions show very good agreement with each other. The EM obtained using coronal abundances does not give consistent values for different lines. However, photospheric abundances seem to provide consistent EMs. The EM distributions show a monotonically increasing trend from $\log T = 5.15 - 6.3$. Of the three theoretical limiting cases we have considered, strong condensation (EM_{con}) best reproduces the observations. Static equilibrium (EM_{con}) does a good job at lower temperatures, but it fails significantly above $\log T = 6.0$. Strong evaporation (EM_{con}) is clearly inconsistent with the observations. We conclude from this that downflows play an important role in powering the moss radiation. A similar conclusion was reached by Bradshaw (2008) on the basis of observed red-shifts (see e.g., Doschek et al. 1976; Brueckner 1981; Klimchuk 1987; Doschek et al. 2008; Del Zanna 2008; Warren et al. 2008; Tripathi et al. 2009).

As we have discussed, one obvious source of downflows is the cooling and draining of plasma that has been impulsively heated by nanoflares. As long as the heated strands have a sub-resolution diameter, this picture is consistent with observations of apparently steady intensities, Doppler shifts, and line widths. Another possible source of downflows is material from Type II spicules. This newly discovered phenomena appears to represent jets of chromospheric plasma that is heated to coronal temperatures as it is ejected (De Pontieu et al. 2007). Presumably the material subsequently cools and falls. Much more observational and modeling work is necessary before any firm conclusions can be drawn.

Although our results support the picture of nanoflares and possibly Type II spicules in the cores of active regions, we cannot rule out steady heating entirely. If magnetic flux strands constrict appreciably at their base, then $EM_{se}(T)$ will have a different shape from that which we have shown (e.g. Warren et al. 2010). The theoretical curve could in principle be brought in line with observations. However, because the transition region is so thin, the constriction must be very dramatic and the transition region must fall right where the constriction occurs. This would seem rather surprising given that the height of the transition region depends on the coronal pressure and moves up and down in response to changes in the heating rate, either slow or rapid. It has been found that the area of quiet Sun network boundaries increases by a factor of about 1.6 between $\log T = 5.4$ and 6.0 (Patsourakos et al. 1999). How this relates to moss regions discussed here is unclear.

The result that photospheric abundances apply in regions of downflow may hold important clues about the origin of the FIP effect, the fractionation of elements based on their first ionization potential. If fractionation (coronal abundances) occurs in regions of steady

heating, where conditions are static, but not in regions of impulsive heating, where there are continual upflows and downflows, then it is suggested that the fractionation process involves some sort of long-term settling. Further observational and modeling work is needed also in this regard.

We thank an anonymous referee for carefully reading the manuscript and comments. DT and HEM acknowledge from STFC. The work of JAK was supported by the NASA Living With a Star Program. We acknowledge the loops IV workshop as an opportunity to stimulate discussions and collaborate on this project. We thank the CHIANTI consortium. We thank Dr Giulio Del Zanna for various discussions and Dr Peter Young for providing his fitting IDL routines in *Solarsoft*. Hinode is a Japanese mission developed and launched by ISAS/JAXA, collaborating with NAOJ as a domestic partner, NASA and STFC (UK) as international partners. Scientific operation of the Hinode mission is conducted by the Hinode science team organized at ISAS/JAXA. This team mainly consists of scientists from institutes in the partner countries. Support for the post-launch operation is provided by JAXA and NAOJ (Japan), STFC (U.K.), NASA, ESA, and NSC (Norway).

REFERENCES

- Antiochos, S. K., et al. 2003, *ApJ*, 590, 547
- Bradshaw, S. 2008, *A&A*, 486, L5
- Bradshaw, S. J. and Cargill, P. J. 2010, *ApJ*, 710, 39
- Bradshaw, S. J. and Cargill, P. J. 2010, *ApJ*, 717, 163
- Bradshaw, S. J. and Klimchuk, P. J. in preparation
- Brooks, D. H. and Warren, H. P. 2009, *ApJ*, 703, 10
- Brosius, J. W., Davila, J. M., Thomas, R. J. and Monsignori-Fossi, B. C. 1996, *ApJS*, 106, 143
- Brosius, J. W., Thomas, R. J., Davila, J. M. and Landi, E. 2000, *ApJ*, 543, 1016
- Brueckner, G. E. 1981, In: *Solar active regions: A monograph from Skylab Solar Workshop III. (A82-19181 07-92)* Boulder, CO, Colorado Associated University Press, 113
- Cargill, P. J. 1994, *ApJ*, 422, 381

- Culhane, J. L., et al. 2007, *Sol. Phys.*, 243, 19
- Del Zanna, G. 2003, *A&A*, 406, L5
- Del Zanna, G. 2008, *A&A*, 481, L49
- De Pontieu, B. et al. 2007, *PASJ*, 59, S655
- Dere, K. P., Landi, E., Mason, H. E., Monsignori Fossi, B. C. and Young, P. R. 1997, *A&AS*, 125, 149
- Dere, K. P., Landi, E., Young, P. R., Del Zanna, G., Landini, M. and Mason, H. E. 2009, *A&A*, 498, 915
- Doschek, G. A., Bohlin, J. D. and Feldman, U. 1976, *ApJ*, 205, 77
- Doschek G. A. et al. 2008, *ApJ*, 682, 1362
- Feldman, U. 1992, *Phys. Scr*, 46, 202
- Feldman, U. and Widing, K. G. 2003, *Space Sci. Rev.*, 107, 665
- Grevesse, N. and Sauval, A. J. 1998, *Space Sci. Rev.*, 85, 161
- Handy, B. N. et al. 1999, *Sol. Phys.*, 187, 229
- Klimchuk, J. A. 1987, *ApJ*, 323, 368
- Klimchuk, J. A. 2006, *Sol. Phys.*, 234, 41
- Klimchuk, J. A., Patsourakos, S. and Cargill, P. J. 2008 *ApJ*, 682, 1351
- Klimchuk, J. A. 2009 in *The Second Hinode Science Meeting: Beyond Discovery-Toward Understanding* (ASP Conf. Ser. Vol. 415), ed. B. Lites, et al. (San Francisco: Astron. Soc. Pacific), p. 221
- Klimchuk, J. A., Karpen, J. T. and Antiochos, S. K. 2010, *ApJ*, 714, 1239
- Landi, E., Feldman, U., & Dere, K. P. 2002, *ApJS*, 139, 281
- Landi, E. and Feldman, U. 2008, *ApJ*, 672, 674
- Landi, E. and Young, P. R. 2009, *ApJ*, 706, 1
- López Fuentes, M. C. and Klimchuk, J. A. 2010, *ApJ*, in press

- Mariska, J. T. and Boris, J. P. 1983, *ApJ*, 267, 409
- Martens, P. C. H., Kankelborg, C. C. and Berger, T. E. 2000, *ApJ*, 537, 471
- O’Dwyer, B., Del Zanna, G., Mason, H. E., Sterling, A. C., Tripathi, D., Young, P. R. 2010, *A&A*, in press
- Parker, E. N. 1988, *ApJ*, 330, 474
- Patsourakos, S., Vial, J.-C., Gabriel, A. H. and Bellamine, N. 1999, *ApJ*, 522, 540
- Patsourakos, S. and Klimchuk, J. A. 2006, *ApJ*, 647, 1452
- Patsourakos, S. and Klimchuk, J. A. 2009, *ApJ*, 696, 760
- Pottasch, S. R. 1963, *ApJ*, 137, 945
- Reale, F., Testa, P., Klimchuk, J. A., and Parenti, S. 2009, *ApJ*, 698, 756
- Sheeley, N. R. Jr. 1995, *ApJ*, 440, 884
- Tripathi, D., Mason, H. E., Young, P. R. and Del Zanna, G. 2008, *A&A*, 481, 53
- Tripathi, D., Mason, H. E., Dwivedi, B. N., del Zanna, G., and Young, P. R. 2009, *ApJ*, 694, 1256
- Tripathi, D., Mason, H. E., Del Zanna, G. and Young, P. R. 2010, *A&A*, 518, xxx
- Warren, H. P. 1999, *Sol. Phys.*, 190, 363
- Warren, H. P. et al. 2008, *ApJ*, 677, 1395
- Warren, H. P., Winebarger, A. R., Brooks, D. H. 2010, *ApJ*, 711, 228
- Warren, H. P., Winebarger, A. R., and Mariska, J. T. 2003, *ApJ*, 593, 1174
- Widing, K. G. 1997, *ApJ*, 480, 400
- Widing, K. G. and Feldman, U. 2001, *ApJ*, 555, 426
- Young, P. R. and Mason, H. E. 1997, *Sol. Phys.*, 175, 523
- Young, P. R., Del Zanna, G., Mason, H. E., Doschek, G. A., Culhane, L. and Hara, H. 2007, *PASJ*, 59, 727
- Young, P. R., Watanabe, T., Hara, H., Mariska, J. T. 2009, *A&A*, 495, 587

Young, P. R. and Landi, E. 2009, ApJ, 707, 173

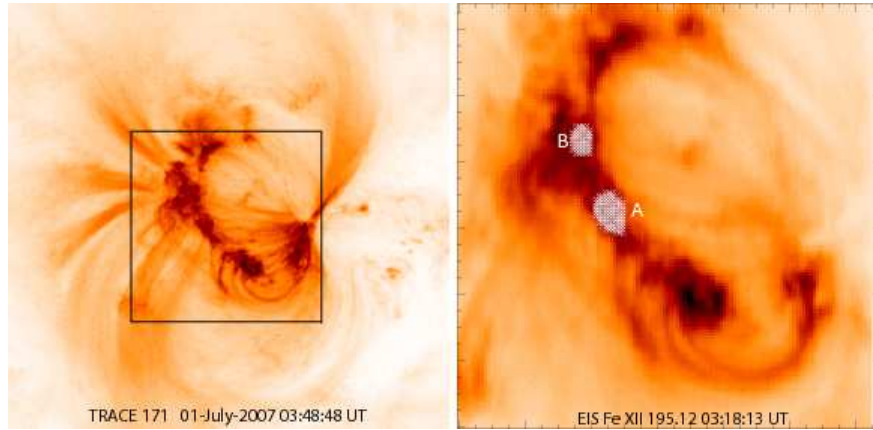


Fig. 1.— Left panel: TRACE 171 Å image showing the complete active region. The overlapped box shows the EIS field of view. Right panel: An image obtained in Fe XII 195.12 Å. The two regions labelled 'A' and 'B' were selected for detailed study.

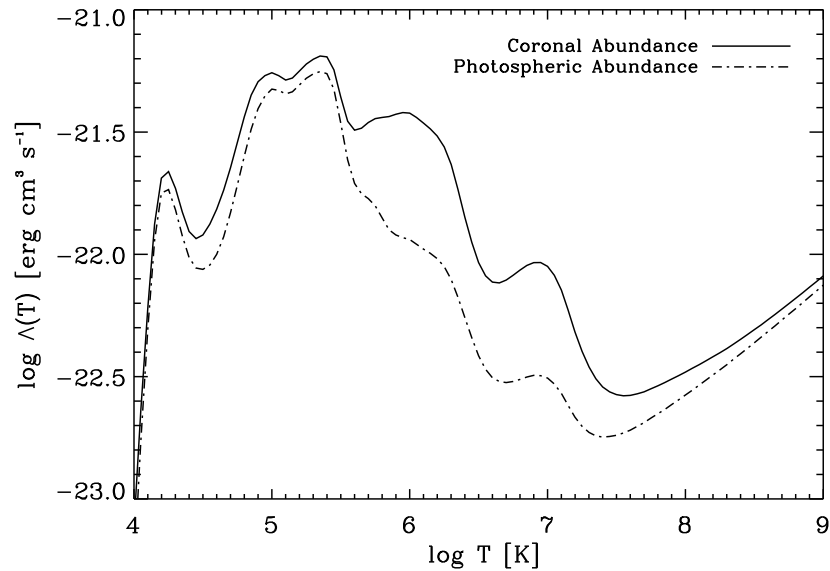


Fig. 2.— Radiative energy losses using the photospheric abundances (dashed-dotted line) of Grevesse and Sauval (1998), coronal abundances (solid line) of Feldman (1992) and CHIANTI v6.0 ionization equilibrium Dere et al. (2009).

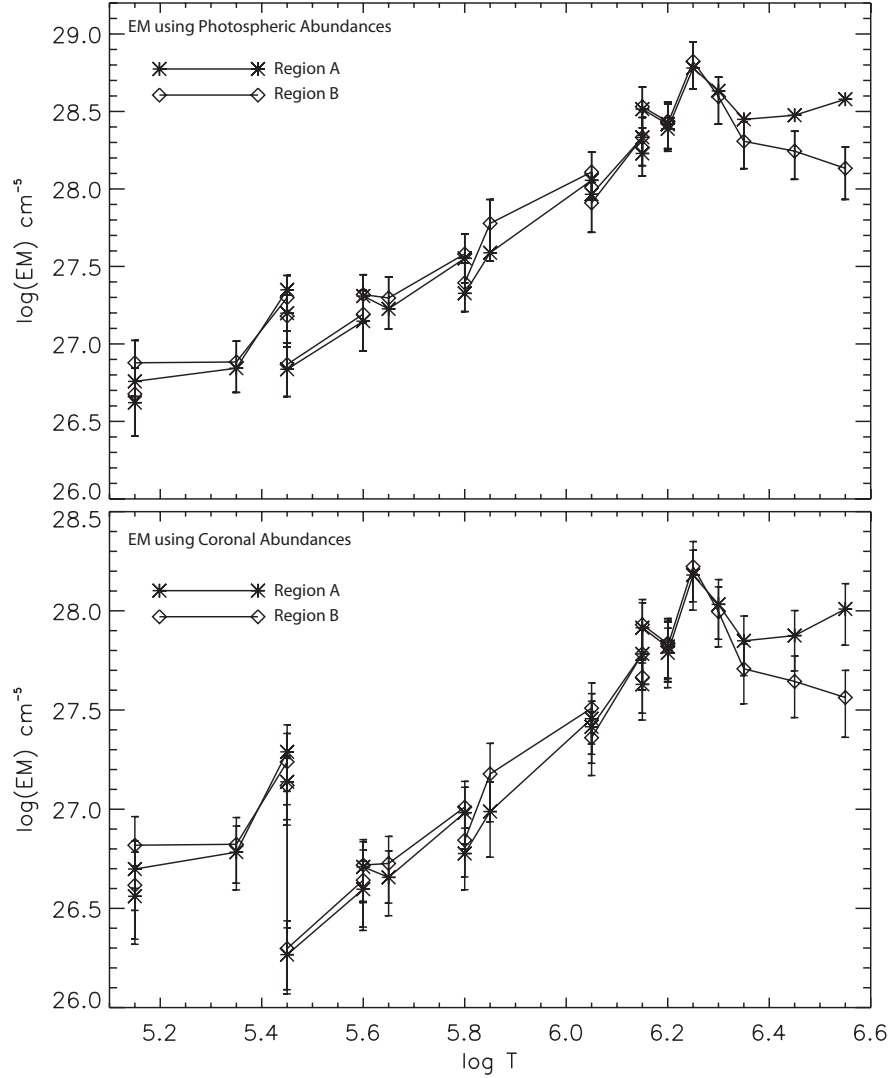


Fig. 3.— Observed EM(T) for two different moss regions A and B shown in the right panel of Fig. 1 using the photospheric abundances (top panel) of Grevesse and Sauval (1998) and the coronal abundances (bottom panel) of Feldman (1992).

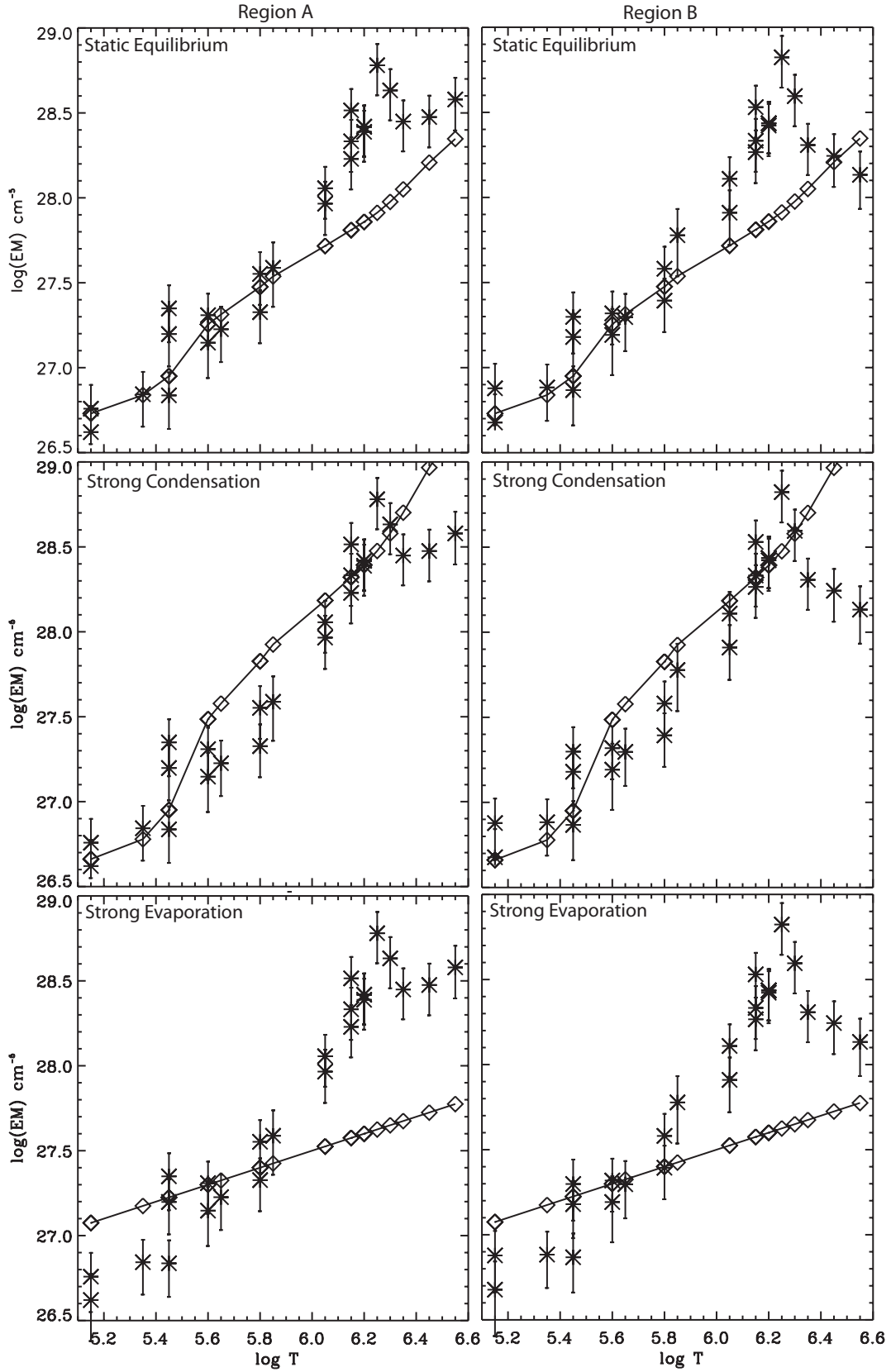


Fig. 4.— Theoretical (solid lines with over-plotted diamonds) EM curve for three limiting cases using Eqns .1, 2 & 3 and observed (asterisks) EM curves using photospheric abundances of Grevesse and Sauval (1998).